DARK MATTER

Dark matter: Do we need it? What is it? Where is it? How much?[1]

16.1 Introduction

The term *'dark matter'* is rather ambiguous, because in its most general sense it simply indicates a mismatch between the amount of matter known (or at least suspected) to be present and the amount of matter we *see* in a given environment or volume. In this sense, matter than emits mostly at infrared wavelengths, such as interstellar dust or brown dwarfs[2] would have qualified as dark matter before the advent of infrared astronomy.

Let us try to be a little more quantitative and return to Table 1.1:

Table 16.1: Cosmic Inventory

Component	$\boldsymbol{\Omega}$ (ρ/ρ_c)
Dark Energy	$\mathbf{0.691 \pm 0.006}$
Matter (baryonic and non-baryonic)	$\mathbf{0.312 \pm 0.009}$
Baryons (Total)	$\mathbf{0.0488 \pm 0.0004}$
Baryons in stars and stellar remnants	$\mathbf{\sim 0.003}$
Neutrinos	$\mathbf{\sim 0.001}$
Photons (CMB)	$\mathbf{5 \times 10^{-5}}$

Comparing the entries in the third and fourth row, we see that stars and their remnants (mostly white dwarfs) account for less than 10% of the

[1] From *"The Dark Matter Rap: Cosmological History for the MTV Generation"* by David Weinberg (http://www.astronomy.ohio-state.edu/∼dhw/Amusements/)

[2] Substellar objects whose core does not reach the high temperatures required to ignite the fusion of H nuclei. You should have encountered brown dwarfs in the *Stellar Structure and Evolution* course.

baryons that make up our Universe, given the value of $\Omega_{\rm b,0}$ deduced from the relative abundances of light elements created in Big Bang Nucleosynthesis (Lecture 8), and from the fluctuations in the Cosmic Microwave Background (Lecture 10). This is evidence for *baryonic dark matter*.

We suspect that most of the *'missing'* baryons may be in the form of intergalactic gas, some of which we see as H I absorption lines in the spectra of distant quasars (Lecture 13). A fraction of this gas may be at high temperatures, $T \sim 10^5$–$10^7\,{\rm K}$, and, if so, it radiates and absorbs light mostly at far-ultraviolet and soft X-ray wavelengths which are difficult to detect—this is the so called WHIM (Warm-Hot Intergalactic Medium). Astronomers are fussy,[3] and strive for a complete and accurate census of all objects of interest, in this case baryons. Hence the on-going efforts to detect the WHIM and to quantify the space density of substellar objects.

In this lecture, however, we will focus on *non-baryonic dark matter*, whose existence is indicated by the finding that $\Omega_{\rm m,0} \simeq 6\,\Omega_{\rm b,0}$ (second and third row in Table 16.1). The term dark matter is of more consequence when applied to non-baryonic dark matter, because in this sense we mean some form of matter that does not interact with electromagnetic radiation, and therefore we'll never be able to see, at least in a conventional sense. And yet, there is a great deal of evidence for the existence of dark matter. In the cases we are going to consider here, the evidence comes from the comparison between gravitational mass and luminous mass on a variety of scales, from galaxies to rich clusters.

16.1.1 Mass-to-Light Ratio

As a convenient measure for comparing gravitational mass with luminous mass on different scales, we use the mass-to-light ratio in the B-band, which encompasses photon wavelengths between $\sim 3800\,{\rm \AA}$ and $\sim 4800\,{\rm \AA}$. The mass-to-light ratio is measured in solar units: ${\rm M}_\odot/{\rm L}_{\odot,{\rm B}}$. Thus, for example, the luminosity of the Milky Way galaxy is estimated[4] to be $L_{\rm MW,B} \simeq 2.3 \times 10^{10}\,{\rm L}_{\odot,{\rm B}}$. If the Milky Way consisted exclusively of solar-type stars we would conclude that it has a mass $M_{\rm MW} \simeq 2.3 \times 10^{10}\,{\rm M}_\odot$.

[3] Well, at least some of them are.

[4] As we view our Galaxy from within, its luminosity is less straightforward to determine than those of external galaxies.

This is of course far too simplistic. Stars are born with a range of masses, and it is the mass that determines both the luminosity and the lifetime of a star. For any reasonable form of the stellar initial mass function,[5] most of the luminosity of a stellar population is contributed by the most massive stars, which have $M/L_{\rm B} \sim 10^{-3}\,{\rm M}_\odot/{\rm L}_{\odot,{\rm B}}$, while most of the mass is in the far more numerous and fainter low-mass stars which can have $M/L_{\rm B} \sim 10^{3}\,{\rm M}_\odot/{\rm L}_{\odot,{\rm B}}$. This is a consequence of the steep dependence of stellar luminosity on mass: $L \propto M^{\sim 3.5}$.

Within 1 kpc of the Sun, the average stellar mass-to-light ratio is found to be:

$$\langle M/L_{\rm B} \rangle \approx 4\,{\rm M}_\odot/{\rm L}_{\odot,{\rm B}} \tag{16.1}$$

As an aside, converting to S.I. units the above mass-to-light ratio corresponds to $\sim 170\,000\,{\rm kg\ watt}^{-1}$; while this may appear very inefficient, recall that the mass of the Sun will support its luminosity for $\sim 10\,{\rm Gyr}$.

In Lecture 6 we saw how the luminosity function (LF) of galaxies is now being determined from ever-increasing samples of galaxies and in different wavelength bands. Integrating the LF of galaxies within hundreds of Mpc from our location, it is found that the total stellar luminosity density in the B-band is:

$$j_{\rm stars,B} = 1.1 \times 10^{8}\,{\rm L}_{\odot,{\rm B}}\,{\rm Mpc}^{-3}\,, \tag{16.2}$$

to which we can therefore associate a mass density:

$$\rho_{\rm stars,B} = 1.1 \times 10^{8}\,{\rm L}_{\odot,{\rm B}} \cdot 4\,{\rm M}_\odot/{\rm L}_{\odot,{\rm B}} \;\approx\; 4.4 \times 10^{8}\,{\rm M}_\odot\,{\rm Mpc}^{-3}\,, \tag{16.3}$$

under the (admittedly rather uncertain) assumption that the typical stellar mass-to-light ratio found within 1 kpc of the Sun applies, on average, to most galaxies. Thus, in units of the critical density $\rho_{\rm c} = 1.36 \times 10^{11}\,{\rm M}_\odot\,{\rm Mpc}^{-3}$ (eq. 1.17), $\Omega_{\rm stars} \approx 3 \times 10^{-3}$, with some degree of uncertainty due to our lack of knowledge of the stellar $M/L_{\rm B}$ in different galaxies.[6]

[5] Again, you will have been introduced to the IMF in the *Stellar Structure and Evolution* course.

[6] Given that stars of different masses not only have widely different different $M/L_{\rm B}$ ratios but also very different lifetimes, the average $\langle M/L_{\rm B} \rangle$ of a galaxy will depend on the ages of its stellar populations.

16.2 Galaxy Rotation Curves

Most of the stars and gas in a spiral galaxy are found within a thin disk that rotates about the centre of the galaxy. With spectroscopy, we can measure the component of the gas and stars velocity projected along the line of sight to us, as a function of location within the disk. On one side of the disk, the stars and gas will appear blueshifted relative to the galaxy systemic velocity, while on the other side they will be redshifted; by tracking the blue/redshift across the galaxy it is therefore possible to determine the rotation speed $v(R)$ of the galaxy as a function of radial distance R from the nucleus. This is commonly referred to as the galaxy rotation curve. Specifically:

$$v(R) = \frac{v_{\rm r}(R) - v_{\rm gal}}{\sin i} = \frac{v_{\rm r}(R) - v_{\rm gal}}{\sqrt{1 - b^2/a^2}} \tag{16.4}$$

where $v_{\rm r}(R)$ is the velocity deduced from the Doppler shift of spectral lines from stars/gas in the disk, $v_{\rm gal}$ is the systemic velocity of the galaxy indicated by the Doppler shift of the nucleus, and $b/a = \cos i$ is the ratio of the minor to the major axis of the ellipse that a disk with inclination angle i to our line of sight projects on the plane of the sky.

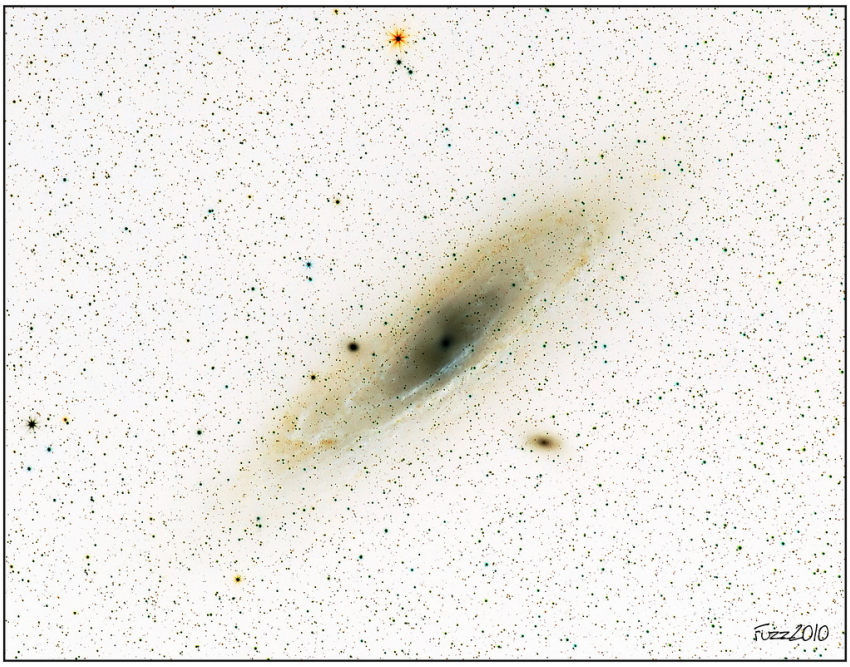

Figure 16.1: M31, the Andromeda galaxy, photographed with a Canon 200 mm telephoto lens. M31 is the nearest major galaxy to the Milky Way.

What behaviour might we expect for the rotation curves of spiral galaxies as we move away from the centre? A star moving in a circular orbit about the nucleus experiences an acceleration:

$$a = \frac{v^2}{R} \tag{16.5}$$

provided by the gravitational attraction of all the matter in the galaxy internal to radius R, so that:

$$a = \frac{G\,M(R)}{R^2} \tag{16.6}$$

Combining the two equations, we can solve for $v(R)$:

$$v(R) = \sqrt{\frac{GM(R)}{R}} \tag{16.7}$$

Thus, the behaviour of $v(R)$ will depend on the functional form of $M(R)$. If the density ρ (g cm^{-3}) of matter within R is constant, then $M = 4/3\pi\rho R^3$ and therefore

$$v(R) \propto R\,. \tag{16.8}$$

For a test particle located at sufficiently large R so that $M(R)$ is constant, we expect

$$v(R) \propto \frac{1}{\sqrt{R}}\,. \tag{16.9}$$

This is often referred to as 'Keplerian rotation', in analogy with the orbits of planets around the Sun, which accounts for 99.8% of the mass of the solar system. Thus, for Keplerian rotation, we expect the rotation speed to *decrease* as we move well beyond the optical dimensions of a galaxy.

Finally, for a distribution of matter in hydrostatic equilibrium, such that $\rho \propto 1/R^2$, the mass contained within a shell of thickness dR at distance R is $M = 4\pi\rho R^2 \mathrm{d}R$, and therefore:

$$v(R) = \text{constant} \tag{16.10}$$

The first galaxy for which the rotation curve was measured out to distances well beyond the optical disk of stars and ionised gas was M31, our closest large galaxy at a distance of 780 kpc. As can be seen from Figure 16.2, the rotational velocity increases from the centre to $v_{\rm rot}^{\rm max} \simeq 255\,{\rm km\ s^{-1}}$ at $R = 8$–$10\,{\rm kpc}$, and then flattens at $v_{\rm rot} \simeq 230\,{\rm km\ s^{-1}}$ out to the limit to

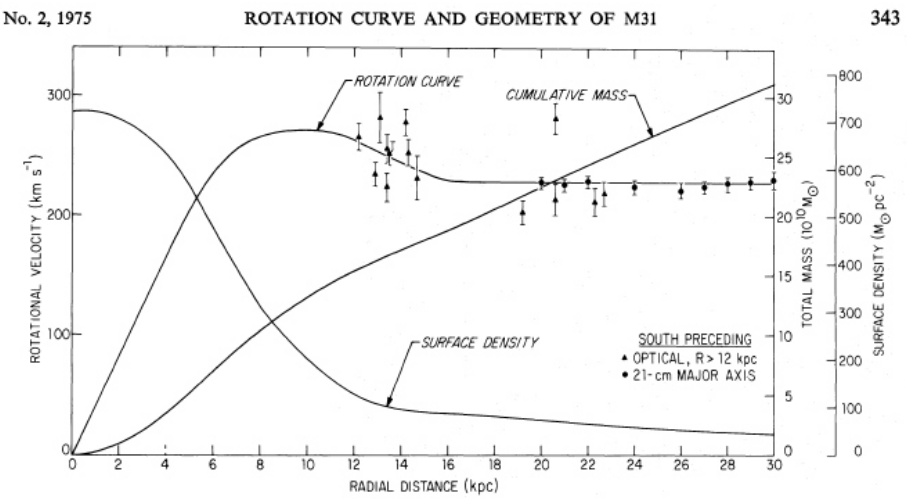

Figure 16.2: The rotation curve of the Andromeda galaxy rises from the centre to $R \simeq 10\,\mathrm{kpc}$, and then remains approximately constant out to $R = 30\,\mathrm{kpc}$, indicating that the mass of M31 continues to increase up to at least that radius. Figure reproduced from Roberts & Whitehurst (1975) who combined their radio observations of the 21 cm emission line of interstellar neutral hydrogen with earlier measurements of nebular emission lines from H II regions by Rubin & Ford (1970).

the data, at $R = 30\,\mathrm{kpc}$. More recent observations have shown that there is still no hint of a drop in v_{rot} out to $R = 40\,\mathrm{kpc}$.

The behaviour exhibited by the M31 rotation curve turns out to be common to most spiral galaxies. In contrast, the integrated stellar light of the disks of spiral galaxies generally falls exponentially with R, that is:

$$I(R) = I(0)\,\exp\left(-\frac{R}{R_{\mathrm{s}}}\right) \tag{16.11}$$

where I is the *surface brightness* (normally measured in magnitudes per square arcsecond) and R_{s} is a characteristic scale-length. For M31, $R_{\mathrm{s}} \simeq 6\,\mathrm{kpc}$. Thus, beyond $20\,\mathrm{kpc}$ ($R > 3R_{\mathrm{s}}$) for example, only $\sim 3\%$ of the light remains, indicating that beyond a few scale lengths the mass of stars inside R becomes essentially constant. In contrast, the gravitational mass enclosed, as indicated by the rotation curve, continues to increase (see Figure 16.2). Clearly, there is dark matter on galactic scales. While some of this dark matter may be baryonic, baryons are unlikely to make up the shortfall. In our own Galaxy and M31, the mass of atomic and molecular gas amounts to only 10–20% of the stellar mass.

Returning to our Galaxy, eq.16.7 can be used to estimate the mass enclosed

within R from the Milky Way flat rotation curve:

$$M(R)_{\rm MW} = 9.6 \times 10^{10}\,{\rm M}_\odot \left(\frac{v}{220\,{\rm km\ s^{-1}}}\right)^2 \left(\frac{R}{8.5\,{\rm kpc}}\right) \tag{16.12}$$

where the scaling is appropriate to the Sun's location in the Milky Way disk. Dividing by the Milky Way luminosity in the B band, we deduce our Galaxy's mass-to-light ratio as a function of distance:

$$\langle M/L_{\rm B}\rangle \simeq 50\,{\rm M}_\odot/{\rm L}_{\odot,{\rm B}} \left(\frac{R_{\rm halo}}{100\,{\rm kpc}}\right) \tag{16.13}$$

So, how far does the Milky Way dark halo extend? As we move to larger distances from the disk, we run out of 'test particles' as stars in the halo become more and more scarce. The furthest the MW halo has been probed with stellar orbits is $R \simeq 50\,{\rm kpc}$. At yet larger distances, we can use arguments based on the motions of satellites orbiting our Galaxy, although with increasing uncertainty. The most recent measurements of relevance to this problem are collected in Figure 16.3, from which the authors conclude that the halo does indeed extend to $\sim 100\,{\rm kpc}$; the best fit to the data indicates a dynamical mass of the Milky Way:

$$M_{\rm dyn}^{\rm MW} \simeq 1 \times 10^{12}\,{\rm M}_\odot\,. \tag{16.14}$$

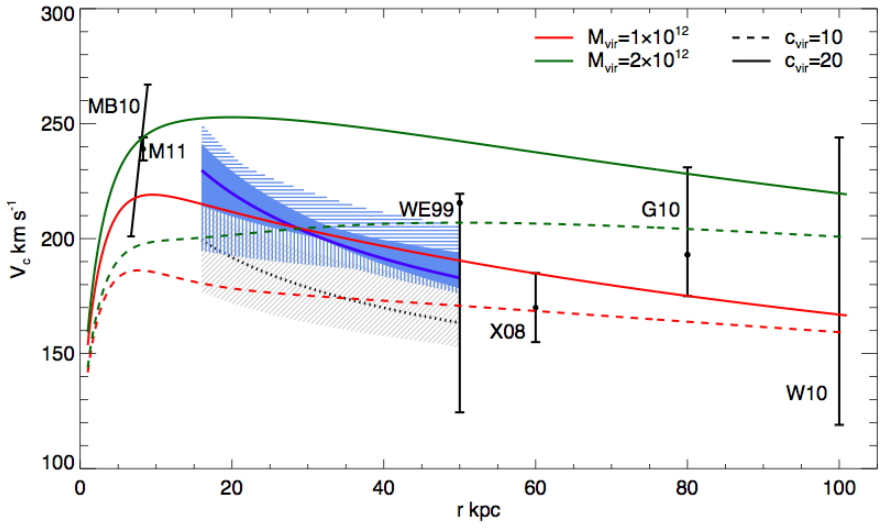

Figure 16.3: The circular velocity profile of the Milky Way galaxy. Data points are labelled with the initials of the authors and the year their measurements were published. The red and green curves show the expectation for $v(R)$ for two values of the dynamical mass of the Milky Way and for two values of a concentration parameter describing the radial distribution of dark matter, as indicated in the top right corner of the plot. (Figure reproduced from Deason et al. 2012).

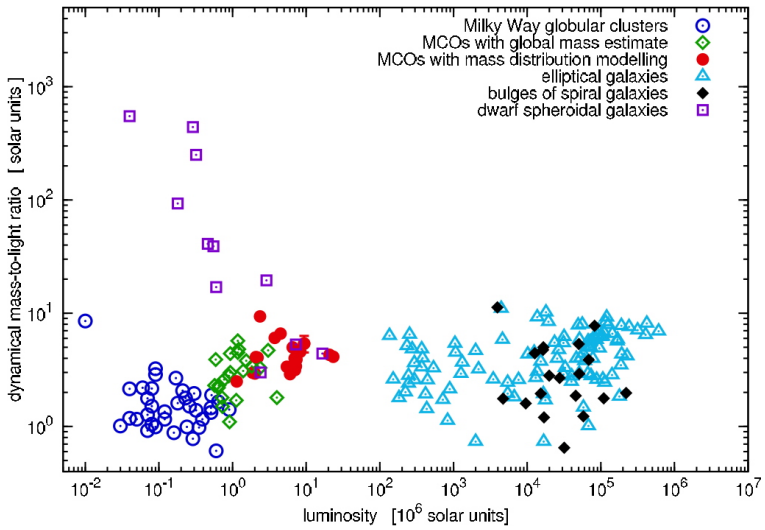

Figure 16.4: Mass-to-light ratio in different galactic environments, as indicated. (Figure reproduced from Dabringhousen et al. 2008).

While some of this mass may be in baryons, it is generally thought that the high values of $M/L_{\rm B}$ implied reflect the fact that the Milky Way disk lies at the centre of a spherical halo of non-baryonic dark matter.

The mass-to-light ratio of a galaxy varies with galaxy type and with location within a galaxy. The inner regions (bulges) of spirals and ellipticals are dominated by baryons. At the other end of the luminosity scale, dwarf galaxies are dominated by dark matter, reaching M/L ratios of several hundred (see Figure 16.4). There is no evidence for dark matter in globular clusters, even though they have the same luminosity as dwarf spheroidal galaxies. The preponderance of dark matter in dwarf spheroidal galaxies (which only harbour old stellar populations) has led to searches for gamma-rays which may be produced by the annihilation of particle-antiparticle pairs of some non-baryonic dark matter candidates. Some results so far have been suggestive, but much remains to be done before astronomical detection of a non-baryonic dark matter signal is established with certainty.

16.3 Dark Matter in Galaxy Clusters

16.3.1 Virial Mass

We have already encountered clusters of galaxies in Lectures 10 and 15. They are the greatest concentrations of matter in the Universe, consisting

of up to $\sim$ 1000 galaxies and $\sim 1 \times 10^{14}$ $M_\odot$ of hot, X-ray emitting gas all moving within the same gravitational potential, provided mostly by the dark matter. By measuring the redshifts of the individual galaxies, it is possible to determine both the systemic redshift of the cluster and the velocity dispersion of its constituents. In *'relaxed'* clusters, that is clusters which have achieved equilibrium and are no longer expanding nor contracting, the velocity dispersion of the galaxies is a measure of the depth of the gravitational potential well within which dark matter, galaxies and intracluster gas move.

The Caltech astronomer Fritz Zwicky is generally acknowledged as being the first to realise that galaxies in the Coma cluster are moving too fast relative to each other to be gravitationally bound by the *luminous* matter within the cluster. He concluded that the cluster must contain dark matter otherwise unaccounted for.

For a system in equilibrium, the virial theorem applies:

$$-2\langle K\rangle = \langle U\rangle \tag{16.15}$$

where K and U are the kinetic and potential energy respectively, and the brackets denote time averages.

Figure 16.5: *Left:* The inner region of the Coma cluster imaged with the Hubble Space Telescope. The cluster lies at a distance of $\sim$ 100 Mpc from our Galaxy. *Right:* Fritz Zwicky, the Swiss astronomer who, while working at Caltech in Pasadena, California during the 1930s correctly deduced the existence of dark matter in the Coma cluster (and other rich clusters of galaxies) from the high velocity dispersion of its galaxies.

For the kinetic energy we can write:

$$K = \frac{1}{2} \sum_i m_i |\dot{\mathbf{x}}_i|^2 \tag{16.16}$$

where m_i is the mass of the ith galaxy, observed at position $\mathbf{x}_i$ within the cluster. The above equation can be re-written as

$$K = \frac{1}{2} M \langle v \rangle^2 \tag{16.17}$$

where $M = \sum_i m_i$ is the mass of all the galaxies in the cluster, and

$$\langle v \rangle^2 \equiv \frac{1}{M} \sum_i m_i |\dot{\mathbf{x}}_i|^2 \tag{16.18}$$

is the mean square velocity (weighted by galaxy mass) of all the galaxies in the cluster.

Similarly, for the potential energy we can write:

$$U = -\frac{1}{2} G \sum_{\substack{i,j \\ j \neq i}} \frac{m_i m_j}{|\mathbf{x}_j - \mathbf{x}_i|} \tag{16.19}$$

where the factor of $1/2$ in front of the double summation ensures that each pair of galaxies is only counted once. An alternative expression for the above is:

$$U = -\alpha \frac{GM^2}{r_\mathrm{h}} \tag{16.20}$$

where α is a numerical factor of order unity that depends on the density profile of the cluster (typically $\alpha \approx 0.4$), and r_h is the half-mass radius, that is the radius of a sphere centred on the centre of mass of the cluster and within which half of the cluster mass is contained. Using (16.15), we therefore have:

$$M \langle v \rangle^2 = \alpha \frac{GM^2}{r_\mathrm{h}} \tag{16.21}$$

from which we can deduce the mass corresponding to a given $\langle v \rangle$ and r_h:

$$M = \frac{\langle v \rangle^2 r_\mathrm{h}}{\alpha G} \tag{16.22}$$

Note the similarity between (16.22) and (16.12) which we used for the Milky Way (or any other spiral galaxy). In both cases, we estimate the mass of a

self-gravitating system by multiplying the square of a characteristic velocity by a characteristic radius (and dividing by the gravitational constant).

Let us apply eq. 16.22 to the Coma cluster, repeating the reasoning by Fritz Zwicky. By measuring the redshifts of hundreds of Coma cluster galaxies, it is found that the mean redshift is $\langle z_{\rm Coma} \rangle = 0.0232$, corresponding to a recession velocity $\langle v_{\rm r} \rangle = c \, \langle z \rangle = 6955 \, {\rm km \ s^{-1}}$ relative to the Milky Way. For $H_0 = 67.5 \, {\rm km \ s^{-1} \ Mpc^{-1}}$, this gives a distance of 103 Mpc.

We can also measure the one-dimensional velocity dispersion of the galaxies, projected along the line of sight to Earth:

$$\sigma_{\rm r} = \Big\langle (v_{\rm r} - \langle v_{\rm r} \rangle)^2 \Big\rangle^{1/2} \ = \ 880 \, {\rm km \ s^{-1}} \tag{16.23}$$

If we assume that the velocity dispersion is isotropic (a reasonable assumption for a relaxed cluster), then the 3D mean square velocity we need in eq. 16.22 is:

$$\big\langle v^2 \big\rangle = 3 \cdot \big(880 \, {\rm km \ s^{-1}} \big)^2 \tag{16.24}$$

The half-mass radius is trickier. All we can do is measure the half-*light* radius and proceed under the assumption that the dark matter (which after all is what we are trying to measure) and the baryons are not segregated within the cluster. In this case, $r_{\rm h} \approx 1.5 \, {\rm Mpc}$. Entering these values in eq. 16.22 and converting throughout to S.I. or cgs units, we find:

$$M_{\rm vir}^{\rm Coma} \approx 2 \times 10^{15} \, {\rm M_\odot} \, . \tag{16.25}$$

More generally:

$$M_{\rm vir} \sim 1.7 \times 10^{15} \, {\rm M_\odot} \left(\frac{\sigma_{\rm r}}{1000 \, {\rm km \ s^{-1}}} \right)^2 \left(\frac{r_{\rm h}}{1 \, {\rm Mpc}} \right) \, . \tag{16.26}$$

For comparison, the total stellar mass of Coma is $M_{\rm stars}^{\rm Coma} \approx 3 \times 10^{13} \, {\rm M_\odot}$, i.e. stars only make up less than 2% of the mass of the cluster. The X-ray emitting intracluster gas contributes $\sim 10\%$, with $M_{\rm gas}^{\rm Coma} \approx 2 \times 10^{14} \, {\rm M_\odot}$. The rest is dark matter. Overall, the mass-to-light ratio measured in Coma is:

$$\left\langle \frac{M}{L_{\rm B}} \right\rangle \approx \frac{2 \times 10^{15} \, {\rm M_\odot}}{8 \times 10^{12} \, {\rm L_{\odot,B}}} \ \approx \ \frac{250 \, {\rm M_\odot}}{\rm L_{\odot,B}} \tag{16.27}$$

i.e. $\sim 5\times$ greater than the $M/L_{\rm B}$ we deduced for the Milky Way (and other spirals).

16.3.2 Hydrostatic Equilibrium

An alternative method to determine the mass of galaxy clusters uses the temperature and density of the hot intracluster gas (see Figure 16.6) which, together with its chemical composition, can be recovered by modelling the continuum (bremsstrahlung) + metal line emission X-ray spectrum of the gas. If the gas is supported by its own pressure against gravitational infall, it must obey the equation of hydrostatic equilibrium:[7]

$$\frac{dP}{dr} = -G\,\frac{M(r)\,\rho(r)}{r^2}\,, \tag{16.28}$$

where P is the pressure, ρ is the density, and M is the total (dark matter + baryons) mass inside a sphere of radius r. For an ideal gas, we also have:

$$P = \frac{\rho k T}{\mu m_{\rm p}}\,, \tag{16.29}$$

where $m_{\rm p}$ is the proton mass and μ is the mean molecular weight, so that the average mass per particle is $\langle m \rangle = \mu\, m_{\rm H}$ ($\mu \simeq 0.6$ for a fully ionised plasma of solar composition).

Combining the last two equations we can solve for the cluster mass:

$$M(r) = \frac{k\,T(r)\,r}{G\,\mu m_{\rm p}}\,\left[-\frac{d\ln\rho}{d\ln r} - \frac{d\ln T}{d\ln r}\right] \tag{16.30}$$

[7] You will have encountered this equation in the *Stellar Structure and Evolution* course.

Figure 16.6: *Left:* The galaxy cluster Abell 383 imaged with the *Hubble Space Telescope* Advanced Camera for Surveys. This cluster is one of the largest concentrations of matter in the local Universe ($z = 0.1887$), with a mass $M \simeq 7.5 \times 10^{14}\,{\rm M}_\odot$. *Right:* The X-ray image of the cluster (shown here superimposed on the *HST* image taken in visible light) obtained by the *Chandra* observatory shows diffuse emission from intracluster gas at temperatures $T \sim 5 \times 10^7\,{\rm K}$.

Thus, by tracking T, ρ and the composition of the cluster gas (which affects μ) from the cluster core to the outskirts, it is possible to deduce the cluster mass. For the Coma cluster, this method gives:

$$M_{\rm hydro}^{\rm Coma} = (1-2) \times 10^{15}\,{\rm M}_\odot \tag{16.31}$$

consistent with the value $M_{\rm vir}^{\rm Coma} \approx 2 \times 10^{15}\,{\rm M}_\odot$ derived in section 16.3.1 (eq. 16.25). The corresponding mass-to-light ratio $M/L_{\rm B} \sim 250\,{\rm M}_\odot/{\rm L}_{\odot,{\rm B}}$ of Coma turns out to be typical of most rich clusters of galaxies.

In Lecture 10.7.1 we discussed the Sunyaev-Zel'dovich effect in clusters of galaxies (see Figure 16.7), and found that the CMB photons intensity decrement is proportional to the integral of the electron density along the line of sight through the cluster:

$$\frac{\Delta I_\nu^{\rm RJ}}{I_\nu^{\rm RJ}} = -2 \int \frac{kT}{m_{\rm e}c^2}\,\sigma_{\rm T}\,n_{\rm e}\,{\rm d}l\,. \tag{16.32}$$

Thus, if we know the mass of the cluster from either virial or hydrostatic arguments, we can calculate the baryon fraction $f_{\rm b}$ of the intracluster gas. Typically, $f_{\rm b} \approx 10-12\%$, confirming the conclusion that non-baryonic dark matter is the dominant contributor to the gravitational potential of clusters.

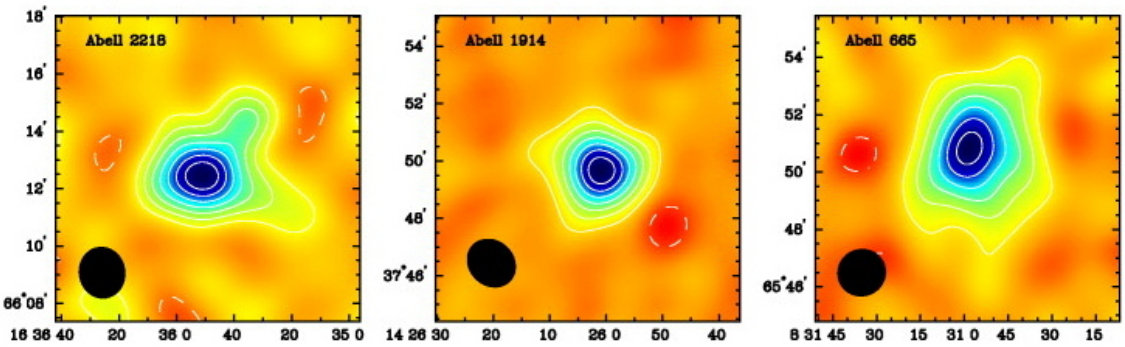

Figure 16.7: Sunyaev-Zel'dovich maps of three clusters of galaxies, showing the temperature difference of the measured CMB relative to the average CMB temperature (or, at a fixed frequency, the difference in radiation intensities). The black ellipse in each image shows the instrumental resolution. For each of the clusters shown here, the spatial dependence of the SZ effect is clearly visible. (Figure reproduced from Grego et al. 2001).

16.4 Gravitational Lensing

16.4.1 Brief History

In Einstein's theory of General Relativity, all mass-energy generates a curvature in its surrounding spacetime. A light ray traversing a region where the gravitational field has a gradient, for example near a point mass, will bend towards the mass. This is *gravitational lensing*, in analogy with conventional optics.

In 1919 Einstein calculated that the positions of stars whose light-rays just graze the surface of the Sun would be displaced from their normal position on the sky by an angle:

$$\alpha = \frac{4G\,\mathrm{M}_\odot}{c^2\,\mathrm{R}_\odot} = 1.7\,\mathrm{arcsec}\,. \tag{16.33}$$

Photographs taken by the Cambridge astronomer Arthur Eddington during the solar eclipse of 29 May 1919 confirmed the GR prediction with an accuracy of $\pm 30\%$, sufficient to establish that the angular shift was twice that expected from Newtonian gravity. Since 1919, eq.16.33 has been verified to within $\sim 0.1\%$: gravitational lensing is not only a prediction of GR, but also a sensitive test of GR.

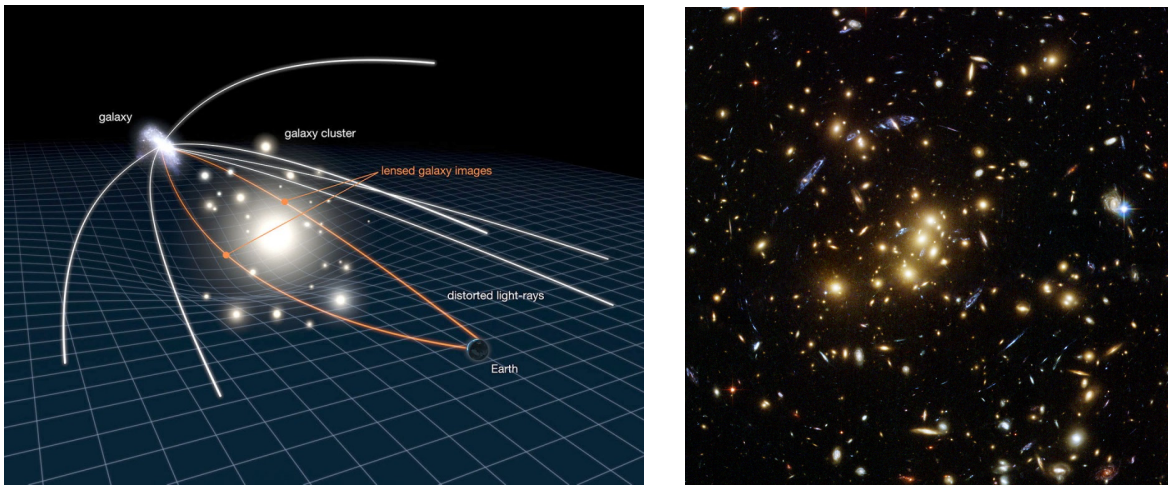

Figure 16.8: *Left:* Schematic representation of gravitational lensing by a galaxy cluster. *Right*: The $z = 0.395$ galaxy cluster Cl0024+1652 imaged with the *Hubble Space Telescope* Advanced Camera for Surveys. With a mass $M = 5 \times 10^{14}\,\mathrm{M}_\odot$, the cluster acts as a gravitational lens: the blue arcs in the *HST* field of view are images of background galaxies at $z \gg 0.395$, stretched and magnified by the curvature of spacetime generated by the mass of the cluster.

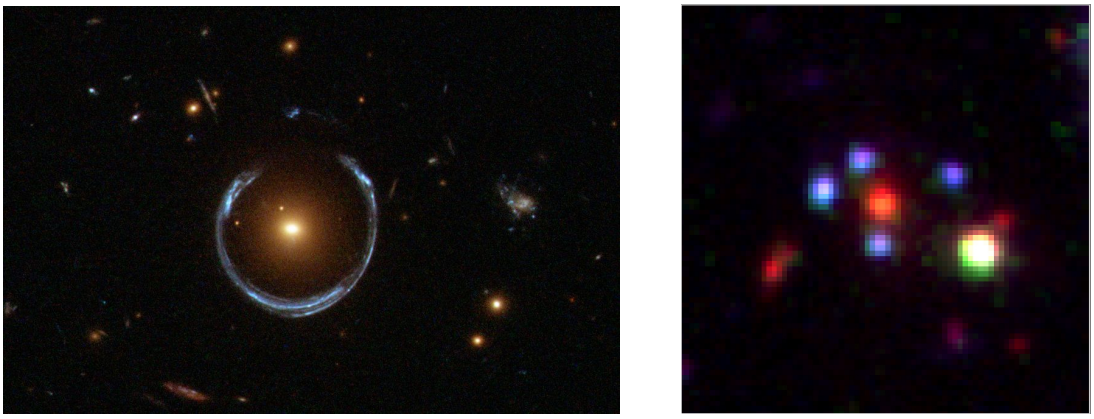

Figure 16.9: *Left: HST* image of the 'Cosmic Horseshoe', a star-forming galaxy at $z = 2.38115$ gravitationally lensed into a near-complete Einstein ring by a foreground massive ($M \sim 6 \times 10^{12}\,\mathrm{M}_\odot$) red galaxy at $z = 0.444$. *Right*: CSWA 20, a blue star-forming galaxy at $z = 1.433$ gravitationally lensed into an Einstein cross (four images) by a foreground massive ($M \sim 4 \times 10^{12}\,\mathrm{M}_\odot$) galaxy at $z = 0.741$. These galaxy-scale gravitational lenses not only give us the means probe the distribution of dark matter in galactic halos, but also allow astronomers to study the physical properties of high redshift galaxies in much more detail than is normally the case (i.e. in the absence of gravitational magnification).

Apart from solar system tests, gravitational lensing remained a theoretical possibility deemed to be beyond experimental verification for sixty years, until the latter part of last century. In the last ~ 30 years, gravitational lensing has grown into a major area of research. Its value is that it allows us to probe the distribution of matter in galaxies and in clusters independently of the nature of the matter, in particular independently of whether the gravitational potential is due to luminous matter or not.

It is customary to distinguish between strong and weak lensing, depending on the projected distance between the light source and the optical axis joining the observer with the mass causing the light deflection, i.e. the lens.

Strong lensing occurs at small angular separations between source and lens. 'Einstein rings', multiple images, highly distorted images and arcs are all examples of strong lensing by either individual massive galaxies or the complex mass distribution of rich clusters of galaxies (see Figures 16.8 and 16.9). The first reported example of strong gravitational lensing was the discovery in 1979 that the quasars 0957+561A,B, separated by 5.7 arcsec on the sky, are two images of the same source at $z = 1.405$. The realisation that the blue arcs often seen in deep images of rich clusters are background galaxies stretched by gravitational lensing followed soon after, in the mid-1980s.

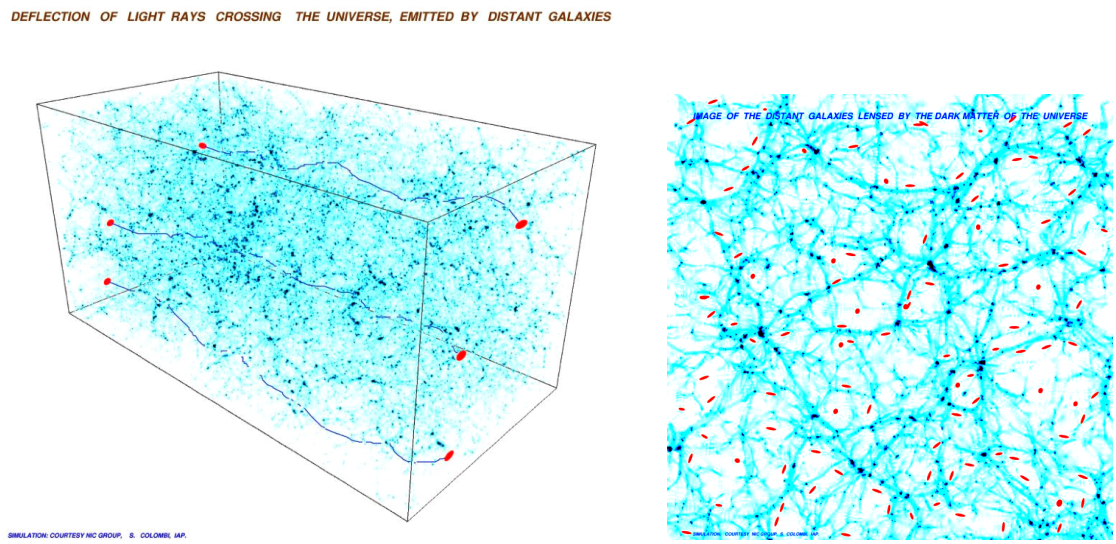

Figure 16.10: Cosmic shear is the weak lensing by the large-scale structure of the Universe. *Left:* Light (shown in dark blue) from distant galaxies (red) is constantly being deflected. *Right*: The observer sees distorted, correlated, images of the distant galaxies. The correlation of their shapes depends on the large-scale structure, and therefore cosmological parameters that determine the evolution of cosmic structure can be extracted from statistical analysis of the distortion pattern.

The magnification afforded by gravitational lensing makes it possible to study distant galaxies in much greater detail than it would otherwise be possible, and even brings within reach of observation galaxies that would otherwise be too faint to detect. Many of the highest redshift galaxies known, at $z > 6$, were identified from their gravitationally lensed images in deep exposures of cluster fields.

Weak lensing occurs when the alignment between observer, lens and source is not close; it produces slightly distorted single images of background galaxies. The large-scale distribution of galaxies in the Universe acts as a weak lens, a phenomenon commonly referred to as *cosmic shear*. Cosmic shear is analysed by statistical means, averaging over many distorted galaxy images. The effect was first reported in 2000, and has been studied since then with the aim of realising its potential as a cosmological tool.

Microlensing is a particular type of strong lensing which occurs when two stars (at the appropriate distances from Earth) become closely aligned as seen from Earth due to their relative transverse velocities. The gravitationally lensed images of the background star are normally too close to be separated, but the event gives rise to a characteristic light curve.

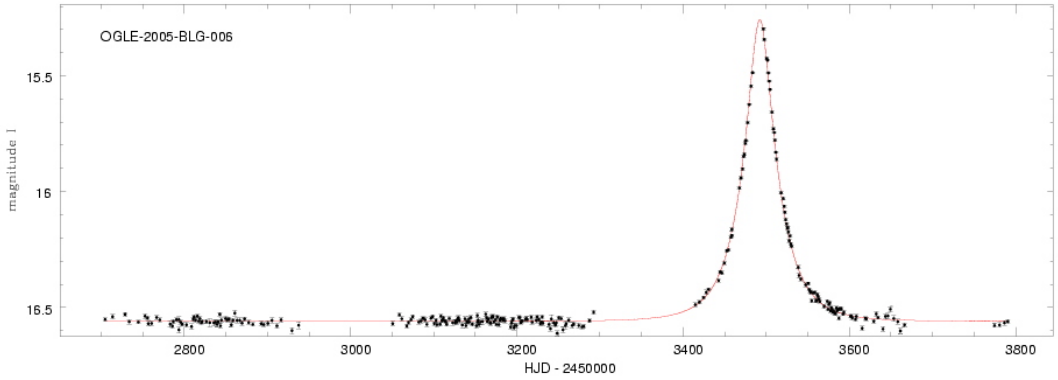

Figure 16.11: Light curve of a microlensing event.

For common lens masses $M_{\rm L} \sim 1\,{\rm M}_\odot$ and typical Galactic velocities, the background source increases in brightness on a timescale of ~ 1 month before returning to its normal (i.e. unlensed) magnitude (see Figure 16.11). A tell-tale sign is that such events are *achromatic*. The first microlensing events in the direction of our companion galaxy, the Large Magellanic Cloud, were reported in 1993.

16.4.2 Gravitational Lensing Basics

In deriving the basic gravitational lensing equations we make some simplifying assumptions. Despite the fact that light rays are affected at some level by all the matter between the light source and the observer (the cosmic shear described above), we shall assume that the lensing action is dominated by a single matter inhomogeneity at some location between source and observer. In the *'thin lens approximation'*, all the action of light deflection takes place at a single distance. We are justified in making this simplification given that the path lengths involved in the halo of a galaxy ($\sim 100\,{\rm kpc}$) and in clusters of galaxies (a few Mpc), are much smaller than the source-lens and lens-observer distances ($\sim$Gpc). Note also that in all the situations considered here the gravitational field is weak, by which we mean that the impact parameter ξ shown in Figure 16.12 is very much greater than the Schwarzschild radius:

$$\xi \gg \frac{2GM}{c^2}\,. \tag{16.34}$$

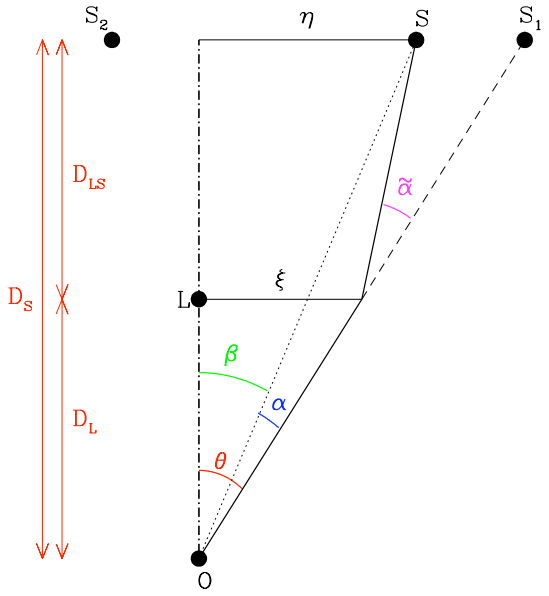

Figure 16.12: Geometry of strong gravitational lensing. In this example, the background source S is seen as two images, S_1 and S_2. The distances indicated on the left-hand side of the diagram are angular diameter distances. Light-rays from S_2 have been omitted for clarity. Note that, in the applications considered here, all the angles in question are small so that, for example, $\theta \simeq \tan\theta = \xi/D_L$.

16.4.2.1 The Lens Equation

With reference to Figure 16.12, in the simplest case where the lens, L, the source S, the image S_1, and the observer O are all in the same plane, the deflection angle is:

$$\tilde{\alpha}(\xi) = \frac{4GM(\xi)}{c^2}\frac{1}{\xi}\,. \tag{16.35}$$

This expression can be derived from the calculation of the photon trajectory in the Schwarzschild metric under the limiting conditions of the thin lens approximation and weak gravitational field. Note that the larger the mass contained with ξ, the larger the deflection; conversely, the larger the impact parameter ξ, the smaller the deflection.

From Figure 16.12 it can be seen that the following relation holds:

$$\theta D_S = \beta D_S + \tilde{\alpha} D_{LS} \tag{16.36}$$

where the distances are *angular diameter distances* and θ, β, $\tilde{\alpha} \ll 1$, a condition that is fulfilled in practically all astrophysically relevant situations. With the definition of the reduced deflection angle as:

$$\alpha(\theta) = \frac{D_{LS}}{D_S}\,\tilde{\alpha}(\theta)\,, \tag{16.37}$$

eq. 16.36 can be expressed as:

$$\beta = \theta - \alpha(\theta) \tag{16.38}$$

In the more general case, when L, S, and O are not all in the same plane (which could be the case for a non-symmetric mass distribution), we treat the angles as vectors on the sky and we obtain the two-dimensional lens equation:

$$\boldsymbol{\beta} = \boldsymbol{\theta} - \boldsymbol{\alpha}(\boldsymbol{\theta}) \tag{16.39}$$

which is the fundamental equation of gravitational lensing.

16.4.2.2 Einstein Radius

For a point lens of mass M, the deflection is given by eq. 16.35. Plugging into 16.38 and using the small angle approximation $\xi = \mathrm{D_L}\theta$, we obtain

$$\beta(\theta) = \theta - \frac{\mathrm{D_{LS}}}{\mathrm{D_L D_S}} \frac{4GM}{c^2\theta} \,. \tag{16.40}$$

In the case where the source is exactly behind the lens, so that $\beta = 0$, we have:

$$\theta_\mathrm{E} = \sqrt{\frac{4GM}{c^2} \frac{\mathrm{D_{LS}}}{\mathrm{D_L D_S}}} \,. \tag{16.41}$$

Note that there is no preferred direction to θ_E: under this special alignment (and in the ideal case of a point mass), a ring-like image is formed (see Figure 16.9) with the Einstein radius θ_E. The angular size of the ring depends only on the mass of the lens and the redshifts of the source and the lens.

θ_E defines the angular scale for a lens situation. In general, if $\beta \lesssim \theta_\mathrm{E}$ lensing produces strong magnification; conversely when $\beta \gg \theta_\mathrm{E}$ there is very little magnification. θ_E can also be the boundary between gravitational lensing producing multiple images (with separations of roughly $2\theta_\mathrm{E}$), or only one image.

Entering the numerical values in eq. 16.41, we have:

$$\frac{\theta_\mathrm{E}}{\mathrm{arcsec}} = \left(\frac{M}{10^{11.09}\,\mathrm{M_\odot}}\right)^{1/2} \left(\frac{\mathrm{D_L D_S/D_{LS}}}{\mathrm{Gpc}}\right)^{-1/2} \,. \tag{16.42}$$

Thus, galaxy-galaxy lensing gives Einstein radii of order ∼arcsec, while galaxy clusters have $\theta_{\rm E} \sim 10$s arcsec. On the other hand, for microlensing of stars in the Galactic bulge by a solar-mass disk star approximately half way to the Galactic centre, we can simplify with $\mathrm{D_{LS}}/\mathrm{D_S} \approx 1/2$:

$$\theta_{\rm E} = 0.64 \times 10^{-3}\,\mathrm{arcsec}\,\left(\frac{M}{\mathrm{M}_\odot}\right)^{1/2}\,\left(\frac{\mathrm{D_L}}{10\,\mathrm{kpc}}\right)^{-1/2}\,, \tag{16.43}$$

i.e. microlensing has a characteristic angular scale of milliarcsec (hence its name).

16.4.2.3 Image Positions and Magnifications

Equations 16.40 and 16.41 can be combined to give the lens equation in terms of the Einstein radius:

$$\beta = \theta - \frac{\theta_{\rm E}^2}{\theta}\,. \tag{16.44}$$

Solving this quadratic equation for the image position θ, one finds:

$$\theta_{1,2} = \frac{1}{2}\,\left(\beta \pm \sqrt{\beta^2 + 4\theta_{\rm E}^2}\right)\,, \tag{16.45}$$

from which it can be seen that an isolated point source always produces *two* images of a background source. The two images are on either side of the source, with one image inside the Einstein ring and the other outside. As the source moves away from the lens (i.e. as β increases), one of the images approaches the lens and becomes very faint, while the other image approaches closer and closer to the true position of the source and tends toward a magnification of unity.

Gravitational lensing magnifies not only the sizes of distant galaxies, but also their fluxes. The reason for this is that lensing conserves surface brightness (flux per unit area on the sky). Then, the magnification of an image is just the ratio between the solid angles subtended by the image and the source, given by:

$$\mu = \frac{\theta}{\beta}\,\frac{d\theta}{d\beta} \tag{16.46}$$

In the symmetric case above, with two images being formed, differentiating

eq. 16.44 gives:

$$\mu_{1,2} = \left(1 - \left[\frac{\theta_{\rm E}}{\theta_{1,2}}\right]^4\right)^{-1} = \frac{u^2+2}{2u\sqrt{u^2+4}} \pm \frac{1}{2}\,, \tag{16.47}$$

where u is the angular separation between lens and source in units of the Einstein radius: $u \equiv \beta/\theta_{\rm E}$.

Note a couple of interesting aspects of the above equation. First, as $\beta \to 0$ (i.e. as the source move towards being exactly behind the lens), the magnification diverges. In the limit of geometrical optics, the Einstein ring of a point source has infinite magnification! Second, for the image inside the Einstein radius, $\theta < \theta_{\rm E}$, its magnification is negative. What this means is that the image has negative parity: it is mirror inverted. A negative μ corresponds to a negative $d\theta/d\beta$ in eq. 16.46: thus, a positive change dβ gives a negative change in dθ, i.e. θ changes in the opposite direction.

The sum of the absolute values of the two image magnifications is the measurable total magnification, μ:

$$\mu = |\mu_1| + |\mu_2| = \frac{u^2+2}{u\sqrt{u^2+4}} \tag{16.48}$$

Note that μ is always larger than one. The difference between the two image magnifications is unity:

$$\mu_1 + \mu_2 = 1\,. \tag{16.49}$$

When the source lies on the Einstein radius, we have $\beta = \theta_{\rm E}$, $u = 1$ and the total magnification becomes:

$$\mu = |\mu_1| + |\mu_2| = 1.17 + 0.17 = 1.34 \tag{16.50}$$

16.4.2.4 Singular Isothermal Sphere

Lensing by a point mass is an idealised situation which obviously does not represent real galaxies. The concept of a singular isothermal sphere (SIS) is the next step in trying to approximate reality. In many galaxies (including spirals with flat rotation curves) the one-dimensional velocity dispersion of

gas and stars, $\sigma_{\rm v}$, is only weakly dependent on distance r from the centre. Treating such a galaxy as 'gas' of stars with pressure $p = \rho kT/m$, where ρ is the density, T the 'temperature' and m the typical stellar mass, we could write $m\sigma^2 = kT$; hence the term 'isothermal', if we take $\sigma_{\rm v}$ to be constant.

A spherical distribution of such stars and gas[8] can be described by the three-dimensional density distribution:

$$\rho(r) = \frac{\sigma_{\rm v}^2}{2\pi G}\,\frac{1}{r^2} \tag{16.51}$$

which has a singularity at $r = 0$, where the density is infinite. A more realistic model has a finite core so that near the centre the density behaves as:

$$\rho = \frac{\rho_{\rm c}}{1 + \left(\frac{r}{r_0}\right)^2}\,, \tag{16.52}$$

where r_0 is the 'core radius'. For $r \ll r_0$, $\rho = \rho_{\rm c}$, while for $r \gg r_0$ the SIS behaviour of eq. 16.51 is recovered.

The SIS model is often used for its simplicity. What we see on the sky is the projection of 16.51 on a plane, which is a circularly symmetric surface mass distribution:

$$\Sigma(\xi) = \frac{\sigma_{\rm v}^2}{2G}\,\frac{1}{\xi}\,. \tag{16.53}$$

The total mass enclosed within a projected distance ξ is:

$$M(\xi) = \int_0^\xi \Sigma(\xi')\,2\pi\xi'\,{\rm d}\xi' \;=\; \frac{\pi\sigma_{\rm v}^2}{G}\,\xi\,. \tag{16.54}$$

Entering this value into eq. 16.35, one obtains the deflection angle for an isothermal sphere:

$$\tilde{\alpha}(\xi) = \frac{4\pi}{c^2}\,\sigma_{\rm v}^2 = 1.4''\,\left(\frac{\sigma_{\rm v}}{220\,{\rm km\ s^{-1}}}\right)^2 \tag{16.55}$$

which is independent of ξ and is only a function of the velocity dispersion. (compare with eq. 16.35 for a point mass). The equivalent expression for

[8]Again, this is an approximation since a realistic galaxy lens usually is not perfectly symmetric but is slightly elliptical. Depending on whether one wants an elliptical mass distribution or an elliptical potential, various modifications of the above formalisms have been suggested.

cored models is:

$$\tilde{\alpha}(\xi) = \frac{4\pi}{c^2}\,\sigma_{\rm v}^2\,\frac{\xi}{(\xi_{\rm c}^2+\xi^2)^{1/2}}\,, \tag{16.56}$$

where $\xi_{\rm c}$ is the core radius.

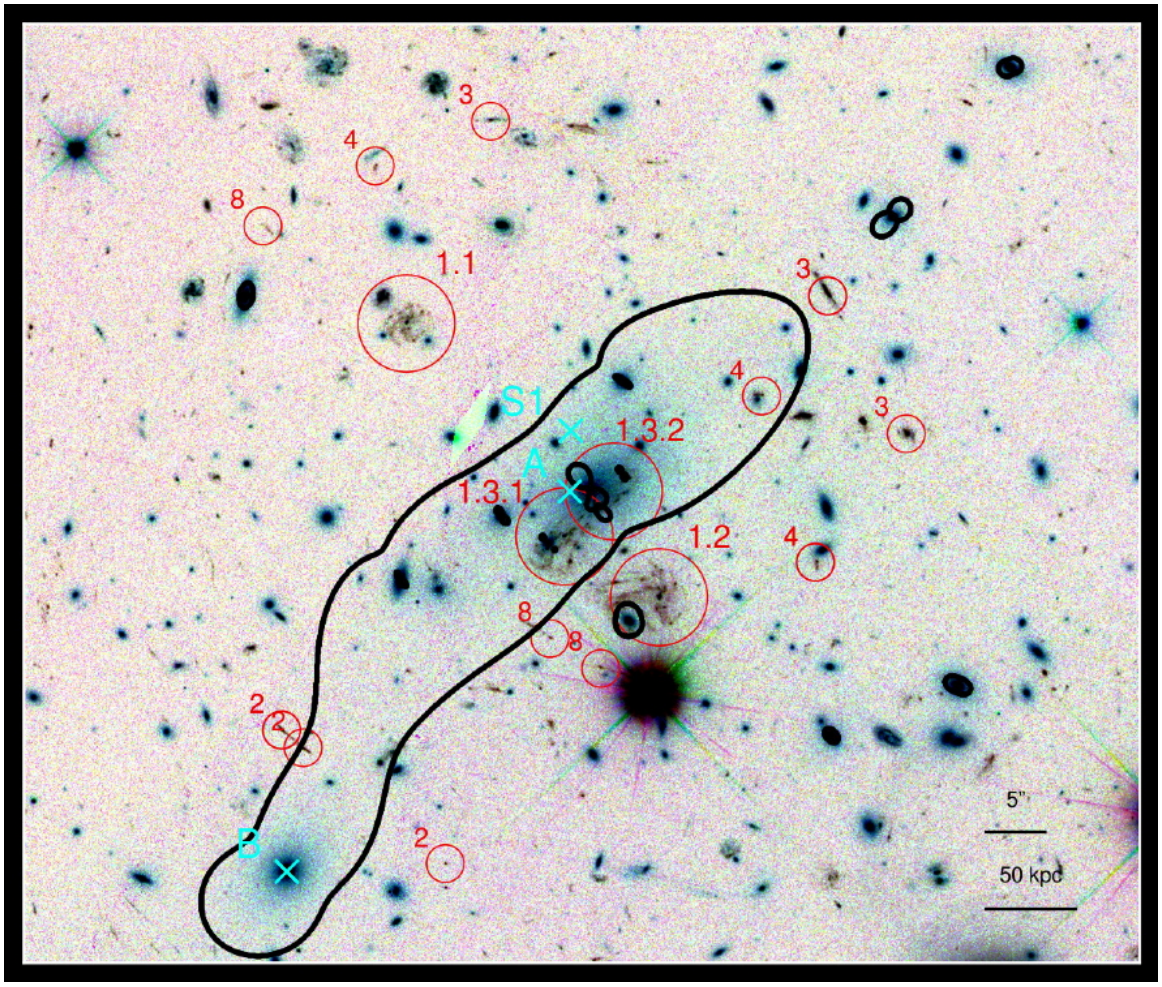

Figure 16.13: *HST* image of the cluster MACS J1149.5+2223. The authors of this study identified five different sources lensed by the cluster in as many as 15 images. The sources are labelled 1, 2, 3, 4 and 8, with 1.1, 1.2, and 1.3 being three images of source 1 (and so on). The source of image system 1 has a spectroscopically determined redshift $z = 1.4906$, while sources 2 and 3 are at $z = 1.894$ and $z = 2.497$ respectively. Sources 4 and 8 have photometric redshifts (deduced from their colours) of $z = 3.0$ and $z = 2.9$ respectively. The cluster is at $z_{\rm cl} = 0.544$. The mass reconstruction places the centre of the dark matter distribution at position A, ~ 1.5 arcsec to the left of the brightest cluster galaxy. (Figure reproduced from Rau et al. 2014).

16.4.3 Conclusions

In the treatment above we have considered image formation by a gravitational lens in the simplest cases. The more complex mass distributions of rich clusters of galaxies are modelled with advanced computational techniques that can use not only the positions but also the surface brightness of multiply lensed images to reconstruct the cluster mass. The large number of images produced by clusters such as that shown in Figure 16.13 allow for well-constrained solutions, once the redshifts of the sources have been determined by spectroscopy or photometry.

In general, the cluster masses deduced by modelling their gravitational lensing effect are in good agreement with the masses found by applying the virial theorem to the motions of the galaxies within the cluster (section 16.3.1), or by applying the equation of hydrostatic equilibrium to the X-ray emitting intracluster gas (section 16.3.2). All three methods arrive at the same conclusion: the gravitational potential of galaxy clusters is dominated by non-baryonic dark matter.

16.5 Epilogue

16.5.1 *Dark Matter: What is it?*

In this lecture we have answered three out of the four questions posed by David Weinberg at the outset. The fourth one still eludes us: we have not yet identified the particle(s) that make up non-baryonic dark matter. There has been, and indeed continues to be, a great deal of speculation about the nature of dark matter. The extent of our ignorance can be gauged by the fact that the masses of candidates proposed span 76 orders of magnitude!

One possibility is a particle that is already known: the neutrino. Although the neutrino was once believed to be massless, there are now indications that it may have a small mass. Neutrinos have been were shown to oscillate between the three known flavors ($\nu_{\rm e}$, ν_μ and ν_τ) that are now described as superpositions of mass eigenstates (ν_1, ν_2, ν_3). Experiments using solar, atmospheric, and reactor neutrinos have measured mass *dif-*

ferences between the three species to be $\Delta m^2_{32} = (2.4 \pm 0.1) \times 10^{-3}\,\mathrm{eV}^2$ $\Delta m^2_{21} = (7.5 \pm 0.2) \times 10^{-5}\,\mathrm{eV}^2$; this requires that at least two mass eigenstates have non-zero mass However, no present-day experiment has the sensitivity to measure the absolute neutrino mass.

The most stringent limit on the sum of the neutrino masses has come from astronomical considerations.[9] Massive neutrinos would affect the way large-scale cosmological structures form (see Lecture 14) by slowing the gravitational collapse of halos on scales smaller than the free-streaming length at the time the neutrinos become non-relativistic. This leads to a suppression of the small scales in the galaxy power spectrum that we observe today. Thus, it possible to infer an upper limit on the sum of neutrino masses by comparing the clustering of galaxies observed in large redshift surveys with the clustering expected for different values of m_ν. By combining the large-scale matter power spectrum with Planck CMB observations,[10] Riemer-Sørensen et al. (2014) derived the most stringent limit yet on the sum of the neutrino masses, $\sum m_\nu < 0.18\,\mathrm{eV}$ (95% confidence limit).

In Lecture 7.2.1 we saw that neutrinos decouple at time $t \sim 1\,\mathrm{s}$, giving rise to a neutrino background that has been propagating through the Universe since redshift $z \sim 10^{10}$. The number density of each neutrino species is 3/11 the number density of CMB photons, so that the total number of neutrinos per unit volume today is:

$$n_{\nu,0} = 3\left(\frac{3}{11}\right) n_{\gamma,0} \;=\; \left(\frac{9}{11}\right) \cdot 4.1 \times 10^2\,\mathrm{cm}^{-3} \;=\; 3.35 \times 10^2\,\mathrm{cm}^{-3} \quad (16.57)$$

with the value of $n_{\gamma,0}$ we deduced in eq. 7.4. The contribution of such a neutrino background to the critical density is:

$$\Omega_{\nu,0}\,h^2 = \frac{\sum m_\nu}{93.14\,\mathrm{eV}}\,. \quad (16.58)$$

Thus, with $\sum m_\nu < 0.18\,\mathrm{eV}$ and $h = 0.675$, we have $\Omega_{\nu,0} < 0.004$. This *upper limit* is comparable to $\Omega_{\mathrm{stars},0}$, and two orders of magnitude lower than $\Omega_{\mathrm{m},0}$. Evidently, relic neutrinos from the Big-Bang are not the main source of non-baryonic dark matter.

[9] Another example of the close connection between astronomy and particle physics.

[10] Massive neutrinos would also have an effect on the primary CMB anisotropies discussed in Lecture 10.

16.5.2 Cold Dark Matter

Neutrinos are an example of hot or warm (depending on their mass) dark matter, as they travel at near relativistic speeds. An alternative class of candidates is Cold Dark Matter, a term meant to indicate particles that decoupled when they were already non-relativistic. Cold dark matter is being given a great deal of attention because its inclusion in hydrodynamic simulations of the growth of structure gives a good match to the observed large-scale distribution of galaxies and voids. Indeed, ΛCDM is the standard paradigm of 21st century cosmology: a Universe whose expansion is now driven by a cosmological constant and in which the energy density of cold dark matter is dominant over other forms of matter, including baryons.

WIMPs (Weak Interacting Massive Particles) are an example of cold dark matter: particles with mass $mc^2 > 10\,\mathrm{GeV}$ (particles of smaller mass would have been detected in particle accelerator experiments) that interact with other particles only through gravity and the weak nuclear force, and are thus intrinsically difficult to detect. Extensions of the standard model of particle physics known as supersymmetry (SUSY) entertain the existence of a large number of new particles, the lightest of which would be stable. None have yet been found in collider experiments, such as the Large Hadron Collider at the European Organization for Nuclear Research (CERN). It must also be said that the supersymmetric WIMP scenario is very uneconomical since it duplicates the standard model with its large number of particles, when actually only one new particle would be needed for dark matter. In any case, the search continues for a WIMP that may fit the astronomical requirements for non-baryonic dark matter.

16.5.3 Modified Physics?

For completeness, we also mention an alternative view to non-baryonic dark matter, held by a minority of astronomers. Rather than appeal to an exotic and hypothetical form of matter whose existence is beyond the standard model of particle physics, some astronomers have proposed that the inflated mass-to-light ratios are an indication that the law of gravity is modified on very large scales. This class of models comes under the general label of *modified Newtonian dynamics* (MOND), first proposed in 1983 by

M. Milgrom.

MOND starts from the premise that Newton's second law, $F = ma$ may not be applicable in the regime of weak acceleration, where it should be replaced by $F = ma^2/a_0$, with $a_0 \simeq 1 \times 10^{-8}\,\mathrm{cm\ s^{-2}}$, comparable to the acceleration of the Sun around the Galactic centre. When $a \ll a_0$, the modified force law leads to flat rotation curves. MOND was developed specifically to explain the flat rotation curves of spiral galaxies, but has subsequently been extended to larger scales. Until a dark matter particle is identified, it will remain a plausible alternative according to some astronomers.